Materials Transactions, Vol. 61, No. 5 (2020) pp. 821 to 827
Special Issue on Materials Science on Mille-Feuille Structure

Loading Orientation Dependence of the Formation Behavior of Deformation Kink Bands in the Mg-Based Long-Period Stacking Ordered (LPSO) Phase

Koji Hagihara[1,*], Takuya Okamoto[1], Ryohei Ueyama[1], Michiaki Yamasaki[2], Yoshihito Kawamura[2] and Takayoshi Nakano[3]

[1]*Department of Adaptive Machine Systems, Graduate School of Engineering, Osaka University, Suita 565-0871, Japan*
[2]*Magnesium Research Center & Department of Materials Science, Kumamoto University, Kumamoto 860-8555, Japan*
[3]*Division of Materials and Manufacturing Science, Graduate School of Engineering, Osaka University, Suita 565-0871, Japan*

The variation in the deformation behavior of a directionally solidified (DS) Mg-based long-period stacking ordered (LPSO)-phase crystal depending on the loading orientation was examined. The frequency of formation of the beak-like shape of the deformation band, which is known as one of the important deformation mechanisms in the LPSO phase, monotonically decreased as the inclination angle of the loading orientation with respect to the crystal growth direction in the DS crystal increased, and was accompanied by a decrease in the yield stress due to the activation of basal slip. Deformation bands formed along a direction approximately perpendicular to the grain boundary independent of the loading orientation. The crystal rotation axes selected in the deformation bands were perpendicular to [0001] in almost all grains, independent of the loading orientation. However, the rotation axes in the bands were not fixed but varied between $\langle 10\bar{1}0\rangle$ and $\langle 11\bar{2}0\rangle$; this variation was correlated with the loading axis. These observed features strongly suggest that the deformation bands formed in the LPSO phase are predominantly deformation kink bands and that the formation mechanism itself does not vary with the loading orientation but instead its details. The selectivity of the crystal rotation axis in the kink band is strongly affected by the loading orientation.
[doi:10.2320/matertrans.MT-MM2019001]

(Received July 3, 2019; Accepted November 20, 2019; Published December 27, 2019)

Keywords: *plastic deformation, long-period stacking ordered phase, magnesium alloy, deformation band, dislocation*

1. Introduction

The so-called long-period stacking ordered (LPSO) phases in Mg alloys are receiving a considerable amount attention for Mg–Zn–Y ternary alloys and some Mg–Zn–RE (RE: rare earth) alloys since these alloys containing the LPSO phase show excellent mechanical properties.[1–16] To clarify the deformation mechanisms of the LPSO phase, we previously examined the plastic deformation behavior of a directionally solidified (DS) LPSO-single-phase crystal.[17–20] As a result, (0001) basal slip was found to be the dominant operative deformation mode, and the formation of a "deformation band" was found to effectively accommodate the plastic strain. Their operation behaviors were assumed to largely vary depending on the loading orientation owing to the anisotropic LPSO crystal structure, but the details have yet not been clarified. In addition, the details related to the nature of the deformation bands and its variation with the loading orientation have not been sufficiently elucidated. It was previously proposed that the deformation bands observed in the LPSO phase are predominately deformation kink bands whose boundaries consist of an array of basal dislocations,[21–27] since the complicated LPSO crystal structure accompanied by the chemical modulation of Zn and RE atoms in particular close-packed planes may prohibit the easy formation of deformation twins. However, the possibility of the formation of deformation twins in the LPSO phase has also been pointed out by some researchers;[28,29] thus, further studies are still required. To address this, we previously examined the crystallographic nature of the deformation bands in the LPSO phase by using a specimen deformed along a direction perpendicular to the basal plane.[23] However, the possibility of variation in the crystallographic nature of the deformation band depending on the loading orientation, the factors controlling the formation behavior of the deformation bands, etc. have not been sufficiently clarified. Given this background, the variations in the deformation behavior and microstructure of an LPSO-phase DS crystal with the loading orientation were examined in this study by compression tests to clarify the abovementioned questions.

2. Experimental Procedure

A mother ingot with a nominal composition of $Mg_{85}Zn_6Y_9$ (at%) was fabricated by induction melting. Using the mother ingot, a directional solidification treatment was conducted using a Bridgman furnace (NEV-DS2, Nissin Giken, Japan) in an Ar gas atmosphere in a carbon crucible at a crystal growth rate of 10.0 mm/h. From observations using transmission electron microscopy (TEM, JEOL JEM-3010), the LPSO phase in the DS crystal was confirmed to have an 18R-type rhombohedral crystal structure, in which the (0001) close-packed plane was stacked 18-fold along the *c* axis. In this paper, the crystal structure of the 18R-LPSO phase is indexed by hexagonal notation by considering a unit cell whose volume is three times larger than that of the rhombohedral cell since this helps to understand the crystallographic nature of the LPSO phase.

The variations in the deformation behavior and microstructure with the loading orientation were examined by compression tests. Rectangular specimens with dimensions of approximately 2 mm × 2 mm × 5 mm were cut by electro-discharge machining. Six different loading axes were chosen. One was set to be parallel to the growth direction; then, the loading axis was tilted in increments of 10° up to 40°. In

*Corresponding author, E-mail: hagihara@ams.eng.osaka-u.ac.jp

addition, a specimen whose loading axis was inclined at 45° with respect to the growth direction was also prepared. Hereafter, these loading orientations are called the 0°, 10°, 20°, 30°, 40°, and 45° orientations. Compression tests were performed at a nominal strain rate of $1.67 \times 10^{-4}\,s^{-1}$ at room temperature (RT) in vacuum. The deformation markings introduced on the specimen surfaces were observed by using optical microscopy (OM, Olympus BX60M) with Nomarski interference contrast. In addition, the variation in the crystal orientation induced by the formation of deformation bands in a specimen was examined by electron backscatter diffraction (EBSD, TSL Solutions K.K.) pattern analysis in a scanning electron microscopy (SEM: JEOL JEM-6500F). The deformation microstructure on the surface whose normal is perpendicular to the growth direction in the DS process was observed for all specimens.

3. Results and Discussion

3.1 Variations in the yield stress and morphology of the deformation bands with the loading orientation

The features of the microstructure of the LPSO phase in the DS crystal grown by the Bridgman method were previously reported in detail in Refs. 17 and 20. The $Mg_{85}Zn_6Y_9$ (at%) crystal was composed almost exclusively of 18R-structured LPSO-phase grains, which show characteristic plate-like shapes whose interfaces are parallel to (0001). Because of the directional solidification treatment, the plate-like LPSO-phase grains were well-aligned along the growth direction, as their (0001) wide interface planes become parallel to it. According to an X-ray diffraction analysis, it was further confirmed that the $\langle 11\bar{2}0 \rangle$ direction was predominantly aligned along the growth direction in many grains.[20] That is, the LPSO phases in the DS crystal exhibit a strong "basal fiber texture" in which the *c* axes in the plate-like grains are all aligned perpendicular to the growth direction and are randomly distributed around the circumferential direction with respect to the growth direction.

Figure 1(a) shows the variations in the yield stress (0.2% offset stress) and work-hardening rate measured at 2% plastic strain as a function of the tilt angle of the loading orientation with respect to the growth direction θ (hereafter referred to as the "tilt angle" for short), and Fig. 1(b) shows the corresponding typical stress–strain curves for compression at RT up to ~5% plastic strain. The highest yield stress of ~150 MPa was observed for the 0° orientation, and the yield stress monotonically decreased as the tilt angle increased to ~40 MPa in the 45° orientation. On the other hand, a low work-hardening rate of ~0.1 GPa was observed for the 0° orientation. This low work-hardening rate was measured just after yielding and continued to ~5% plastic strain, as shown in Fig. 1(b). A stress–strain curve with similar features including the low work-hardening rate was continuously measured up to $\theta = 20°$. At $\theta = 30°$, although a low work-hardening rate was observed just after yielding, it rapidly increased above ~1.5% plastic strain, and the work-hardening rate at 2% drastically increased to ~1.1 GPa. In the specimen with $\theta = 40°$, a high work-hardening rate was measured just after yielding, and the work-hardening rate at 2% showed a similar high value as that measured for $\theta = 30°$. The high work-hardening rate was maintained up to $\theta = 45°$. These features of the variation in the work-hardening rate strongly suggest that the mechanism controlling the deformation drastically varies at around $\theta = 30°$.

To examine the origin of the variations in the mechanical properties as a function of the tilt angle, Figs. 2(a)–(f) show the typical examples of the morphologies of the deformation microstructures introduced in the specimens deformed up to ~5% plastic strain. As previously reported, in the specimen deformed in the 0° orientation, a large number of deformation bands, which are thought to be deformation kink bands, were introduced.[20] The areal fraction of formed deformation bands with respect to the entire specimen surface was quantitatively evaluated by a two-contrast image analysis using ImageJ software[30] and is plotted in Fig. 3. The number of formed deformation bands monotonically decreased as the tilt angle increased. The areal fraction of deformation bands observed for the 5% plastic strain specimen was ~40% in the 0° orientation, while it was as small as ~2% in the 45° orientation. For specimens in which the loading orientation

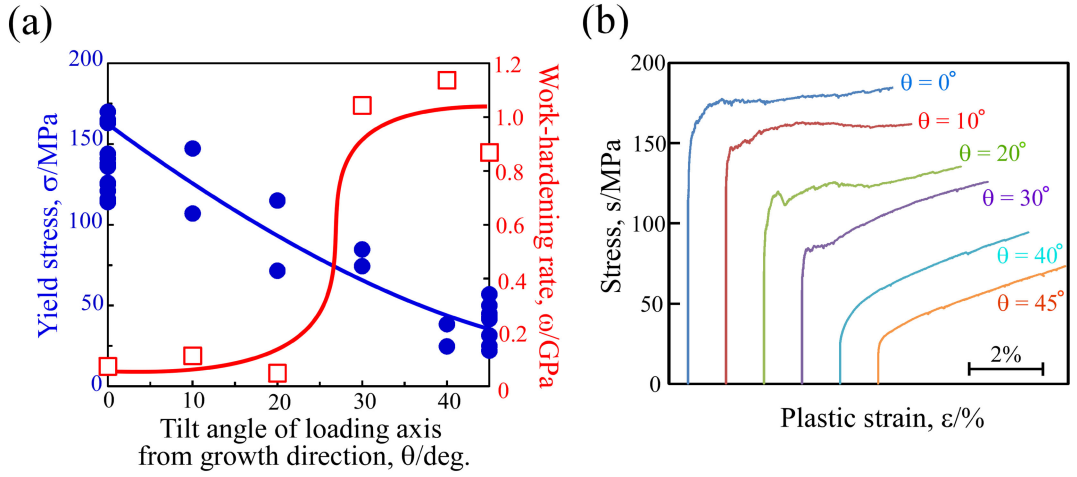

Fig. 1 (a) Variations in the yield stress (0.2% offset stress) and work-hardening rate measured at 2% plastic strain as a function of the tilt angle of the loading orientation with respect to the growth direction. (b) Corresponding typical stress–strain curves for compression at RT up to ~5% plastic strain.

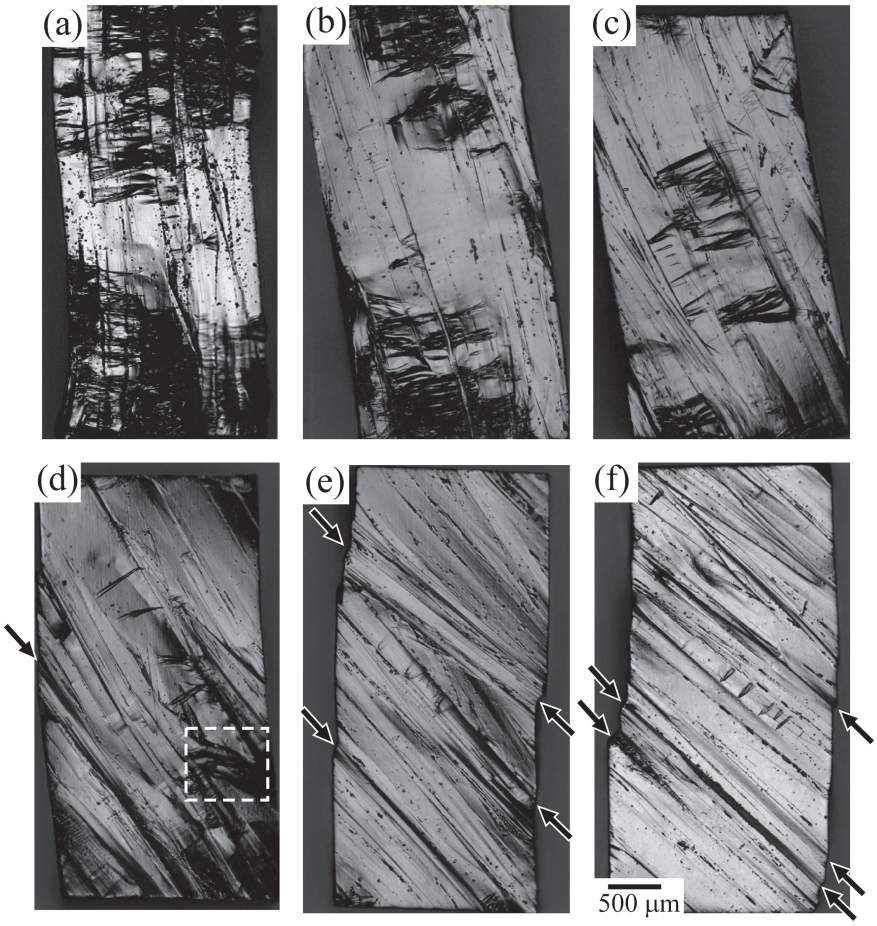

Fig. 2 OM images of the specimens deformed up to ~5% plastic strain at RT in the (a) 0°, (b) 10°, (c) 20°, (d) 30°, (e) 40°, and (f) 45° orientations.

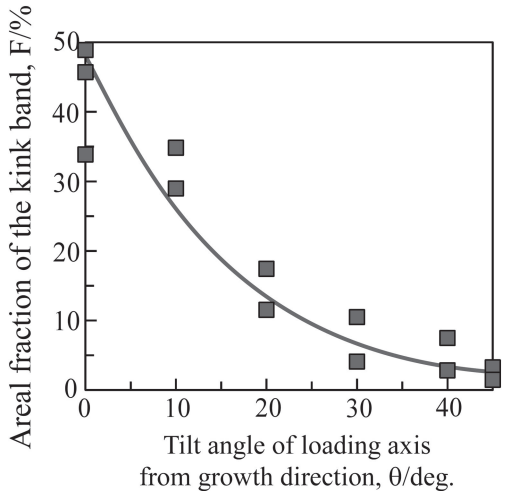

Fig. 3 Variation in the areal fraction of formed deformation bands with respect to the entire specimen surface as a function of the loading orientation measured in specimens compressed at RT to ~5% plastic strain.

was largely inclined with respect to the growth direction, a large number of fine slip traces were introduced in the grains instead of the deformation bands. The microstructural observation results suggest that this transition in the predominant deformation mechanism occurs at around $\theta = 30°$, which is in good agreement with the drastic variation in the work-hardening rate observed at $\theta = 20°$–$30°$ (Fig. 1(a)). According to the previous analysis focused on the 45°-oriented specimen, the fine slip traces were confirmed to be derived from (0001)$\langle 11\bar{2}0\rangle$ basal slip.[17–20,31] Since the plate-like interface of LPSO-phase grains is known to be parallel to the (0001) basal plane, an increase in the tilt angle induces an increase in the Schmid factor for (0001) basal slip in some of the grains. This must be the origin of the monotonic reduction in the yield stress as the tilt angle increases. Indeed, it was observed that the introduction of basal slip was significantly concentrated in some of the grains that are thought to have larger Schmid factors compared to other grains, resulting in the formation of a large step on the specimen surface, as indicated by the arrows in Figs. 2(d), (e) and (f).

It was previously reported that for deformation in the 0° orientation, the deformation bands frequently show characteristic beak-like (ridge-like) shapes, and macroscopically, they tend to develop along a direction nearly perpendicular to the loading orientation.[17–20] This is confirmed in Fig. 2(a). However, the variations in such features with the loading orientation have not yet been reported. This was examined in the analysis of the deformation microstructure in Figs. 2(a)–(f). Figure 4(a) shows the variations in the angle between the elongation direction of a deformation band and the loading orientation (α), the angle between the elongation direction of a deformation band and a grain boundary (β), and the angle

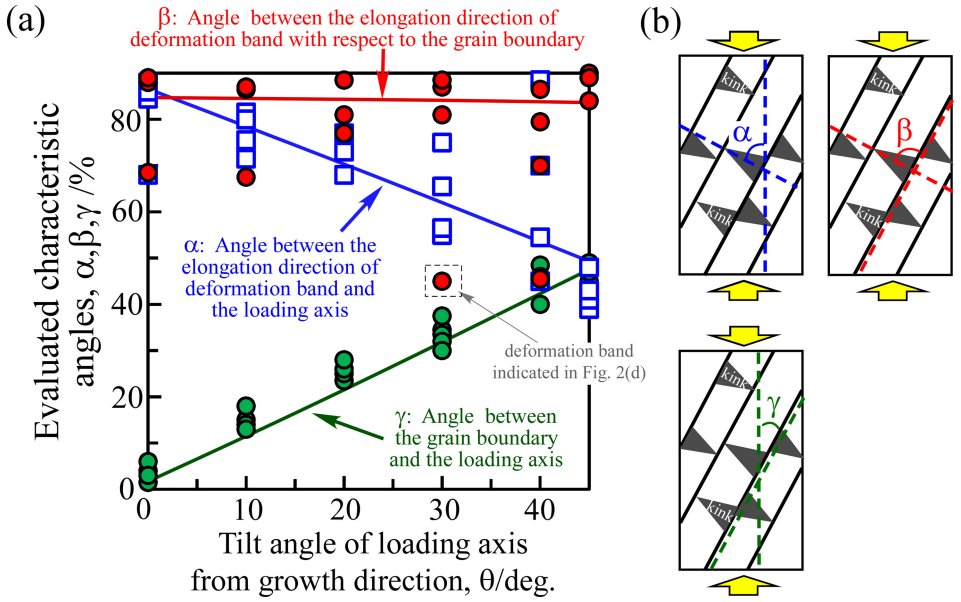

Fig. 4 (a) Variations in the angle between the elongation direction of the deformation band with respect to the loading axis (α), the angle between the elongation direction of the deformation band with respect to the grain boundary (β), and the angle between the grain boundary and the loading axis observed on the specimen surface (γ). (b) Schematic showing the definitions of α, β, and γ.

between a grain boundary and the loading axis observed on a specimen surface (γ). The definitions of these angles are indicated in the schematic in Fig. 4(b). Although there is a small amount of scatter of ~10° due to disturbances in the texture of the DS crystal, γ almost linearly increased as the tilt angle increased from 0° to 45°, which demonstrates that the specimens were well-prepared, as expected. Focusing on α, it monotonically decreased from ~90° to ~45° as the tilt angle θ increased from 0° to 45°, while β was almost constant at around 90°, independent of θ. This obviously demonstrates that the deformation bands are almost always introduced perpendicular to the grain boundary irrespective of the loading orientation. It is noted that a small number of deformation bands that were not elongated in the direction perpendicular to the grain boundary exist; one example is indicated by the gray arrow in Fig. 4(a). The corresponding deformation bands are indicated by the white dashed rectangle in Fig. 2(d). Most of the deformation bands showed characteristic beak-like shapes, but the deformation bands elongated in different directions showed a different wavy shape.

Figure 5 shows the corresponding inverse pole figure (IPF) map, i.e., the crystal orientation map, of such a wavy deformation band examined by SEM-EBSD. In the map, a boundary with a misorientation angle of more than 5° was regarded as a grain boundary and drawn with a black line. It was found that such wavy-shaped deformation bands are always observed in grains whose surface normals are close to [0001], which are colored in red in the crystal orientation map. In a previous study using a specimen deformed in the 0° orientation, we speculated the three-dimensional structure of the deformation band as shown in Fig. 5(b).[25] That is, in many cases, two deformation bands are simultaneously formed, and their combination develops the beak-like morphology. They macroscopically propagate along a direction perpendicular to the basal plane but exhibit a wavy shape only on (0001). The physical origin for the occurrence of this wavy morphology was discussed from the viewpoint of the specific arrangement of basal dislocations with different Burgers vectors on the deformation band boundary.[32] The present results demonstrate the validity of the deformation band model in Fig. 5(b) and further suggest that the same features of the deformation bands are developed independent of the loading orientation for the LPSO phase.

This detected feature—the macroscopic propagation of deformation bands only along one direction that is perpendicular to the grain boundary irrespective of the loading axis—is largely different from that observed in deformation twins. Kishida *et al.* previously proposed the possibility of the formation of a $\{11\bar{2}1\}$ twin in a Mg–Gd–Al alloy containing the LPSO phase.[28] In the case of the $\{11\bar{2}1\}$ twin, six equivalent $\{11\bar{2}1\}$ planes, i.e., $(11\bar{2}1)$, $(11\bar{2}\bar{1})$, $(1\bar{2}11)$, $(1\bar{2}1\bar{1})$, $(2\bar{1}\bar{1}1)$, and $(2\bar{1}\bar{1}\bar{1})$, are possible as the twin habit plane; thus, several different deformation trace angles should be observed in the deformation bands depending on the loading axis. The fact that such trace angles were not observed in the present results suggests that the deformation bands formed in the $Mg_{85}Zn_6Y_9$ 18R-LPSO phase are predominately deformation kink bands.

3.2 Variations in the crystallographic nature of the deformation band with the loading orientation

Regarding the crystallographic features of the deformation bands for the LPSO phase, we previously examined them by using a specimen deformed in the 0° orientation via SEM-EBSD analysis. As a result, we found that the deformation bands in the LPSO phase show the following arbitrariness regarding their crystallographic nature.[23] First, the crystal rotation angle is not fixed and shows a relatively wide distribution. Second, the crystal rotation axis is always perpendicular to [0001] but ambiguously varies on the [0001] zone axis from band to band. On the basis of these findings,

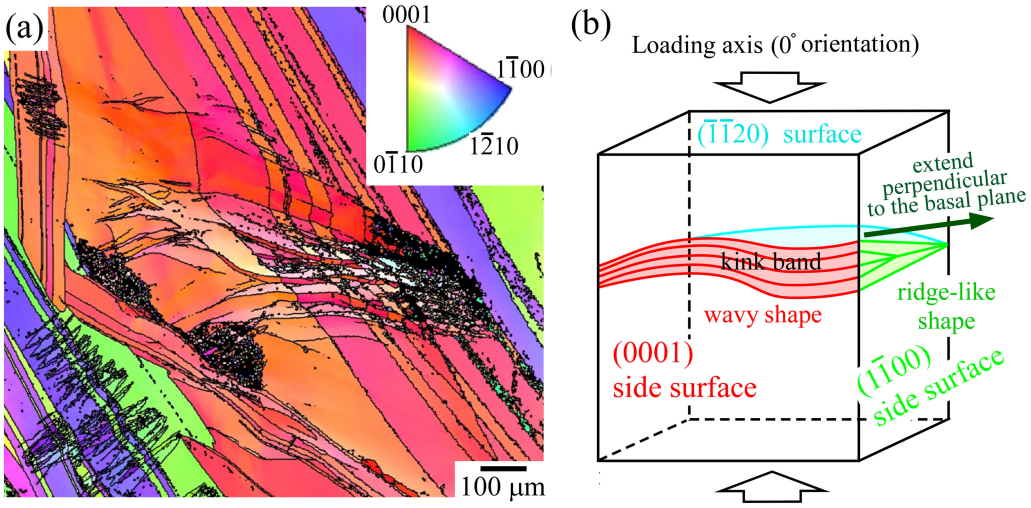

Fig. 5 (a) Typical example of a crystal orientation map of the wavy-shaped deformation band acquired by SEM-EBSD. The observed specimen was deformed in the 30° orientation to ~5% plastic strain. (b) Three-dimensional structure of the deformation band speculated in a previous study that analyzed a specimen deformed in the 0° orientation.[25)]

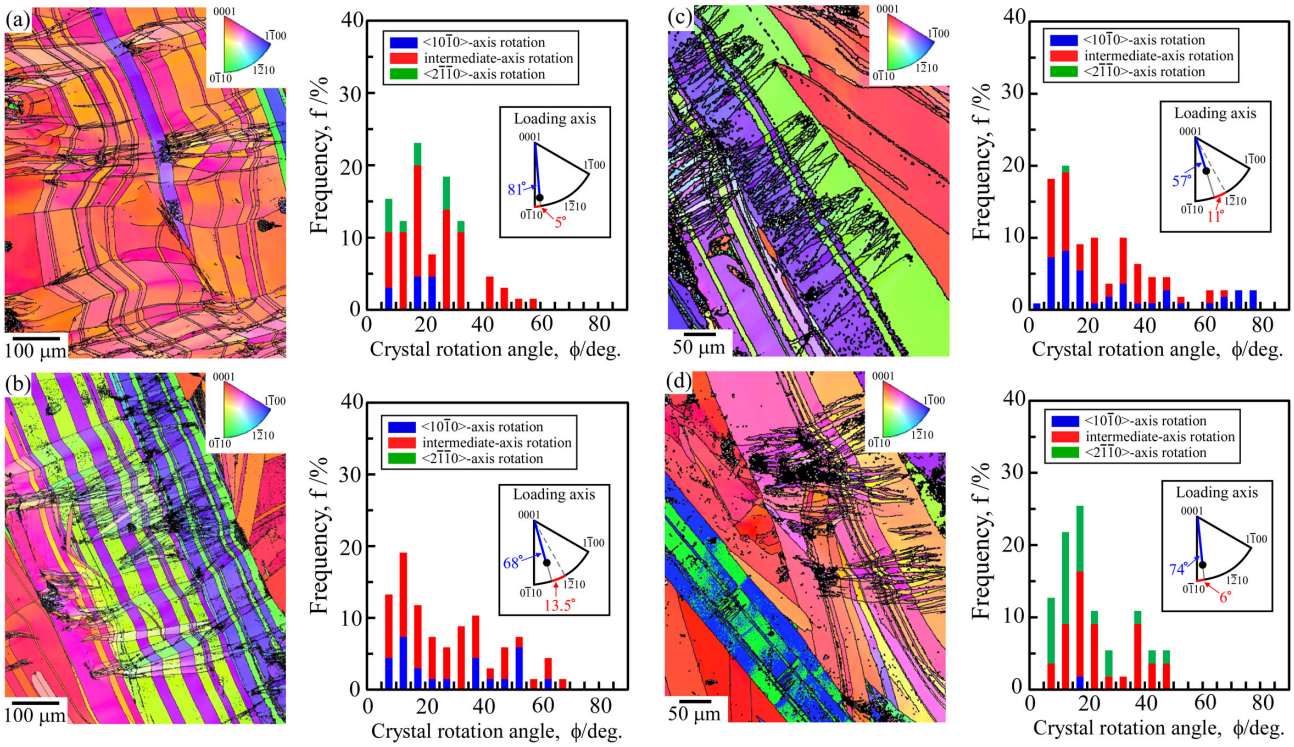

Fig. 6 Typical IPF maps showing the variation in the crystal orientation caused by the formation of deformation bands in specimens deformed in the (a) 10°, (b) 20°, (c) 30°, and (d) 40° orientations to ~5% plastic strain. In addition to the IPF maps, the distribution of the rotation angle of the crystal orientation in the deformation bands in the observed grains is plotted as a bar graph. In the bar graphs, the proportions of the measured rotation axes in the deformation bands are indicated by the different colors. The tolerance of the deviation in the angle for the ⟨10$\bar{1}$0⟩ and ⟨2$\bar{1}\bar{1}$0⟩ rotation axes was set to be within 5°.

we examined whether or not there exist variations in the crystallographic nature of the deformation kink bands depending on the loading orientation in this study. Figures 6(a)–(d) show the typical IPF maps showing the variation in the crystal orientation due to the formation of deformation bands in the specimens deformed in the 10°, 20°, 30°, and 40° orientations, respectively. In addition to the IPF maps, the distribution of the rotation angle in the deformation bands in the observed grains is plotted as a bar graph in increments of 5°. Further, the rotation axes in the deformation bands were also examined, and their variations are indicated by the different colors in the bar graphs. The definitions of the rotation angle and axis in the deformation band are indicated in Fig. 7. In each graph, the corresponding loading orientation in the measured grain is indicated by the stereographic projection, and the angles between the [0001] *c* axis or ⟨1$\bar{2}$10⟩ *a* axis and the loading orientation are also indicated. Note that in the specimens deformed in the 10°,

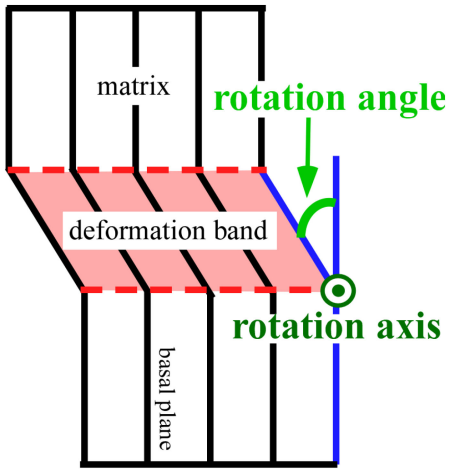

Fig. 7 Schematic showing the definitions of the rotation angle and axis in a deformation band, as analyzed in Fig. 6.

20°, and 30° orientations, the grain in which deformation bands formed could be easily found, and the misorientation angle between the loading axis and the *c* axis in the grain is nearly comparable to the value of 90° – θ (tilt angle). In the specimen deformed in the 40° orientation, however, no such grain could be found. In all of the grains in which deformation bands formed, the angle between the loading orientation and the *c* axis was more than 90° – θ. That is, the deformation band selectively formed in the grain in which the loading orientation is very far from the [0001] axis. This is because of the easy operation of basal slip in the predominantly existing nearly 40°-inclined grains; thus, the formation of deformation bands was limited in such few grains.

As shown in Fig. 6, the crystal rotation angle exhibited a wide variation for all specimens, and no tendency was observed for this variation depending on the tilt angle of the loading axis. Concerning the crystal rotation axis, almost all of them are perpendicular to the [0001] *c* axis, and few deformation bands having a rotation axis containing a *c* component beyond a deviation angle of 5° were found. However, the rotation axis widely varied on the [0001] zone axis for all specimens. The deformation bands whose rotation axes were parallel to $\langle uvt0\rangle$, which were apart from both $\langle 10\bar{1}0\rangle$ and $\langle 2\bar{1}\bar{1}0\rangle$ by more than 5°, were most frequently observed, as indicated by the red bars, but some deformation bands with a rotation axis near $\langle 10\bar{1}0\rangle$ and $\langle 2\bar{1}\bar{1}0\rangle$ (colored blue and green) were also observed. It is emphasized that such a distribution of the crystal rotation axis on the [0001] zone axis was not correlated with θ in the compression test, but it was strongly affected by the misorientation angle between the loading axis orientation and the $\langle 1\bar{2}10\rangle$ direction in the deformed grain. That is, for the grains shown in Figs. 6(a) and (d) in which the loading axis was close to $\langle 0\bar{1}10\rangle$, the relative number of deformation bands with a crystal rotation axis near $\langle 2\bar{1}\bar{1}0\rangle$ increased. In contrast, for the grains shown in Figs. 6(b) and (c) in which the loading axis was close to the $\langle 1\bar{2}10\rangle$, the relative number of deformation bands with a crystal rotation axis near $\langle 10\bar{1}0\rangle$ increased. This feature is in good agreement with that observed for the deformation kink bands formed in a Zn single crystals,[32] and those formed in the LPSO phase deformed at 0° orientation.[23] With the help of a computational analysis based on a finite-element crystal plasticity method, it was clarified that this variation in the crystal rotation axis depending on the loading axis for the Zn single crystal is brought about by the variation in the type of basal dislocations that form the deformation kink band boundaries.[32] In the Zn single crystal whose loading axis is near $\langle 1\bar{2}10\rangle$, basal dislocations with a Burgers vector parallel to $\langle 1\bar{2}10\rangle$ are frequently activated and form a kink band boundary. However, in a single crystal whose loading axis is near $\langle 0\bar{1}10\rangle$, basal dislocations with Burgers vectors parallel to $\langle 1\bar{2}10\rangle$ and $\langle \bar{1}\bar{1}20\rangle$ are activated at a comparable frequency, and both of them form the kink band boundary. According to the kink band formation model proposed by Hess and Barrett, the crystal rotation axis in the deformation kink band is set to be the direction perpendicular to both the (0001) slip plane normal and the shear direction of the basal dislocation.[21] This accounts for the abovementioned experimental results obtained for the Zn single crystal well.[32] The fact that a similar feature for the variation in the crystal rotation axis with the loading orientation is observed for the LPSO phase independent of the tilt angle also supports the conclusion that the deformation bands formed in the LPSO phase are predominately deformation kink bands. The present results demonstrate that the formation mechanism of the deformation kink band itself does not vary depending on the loading orientation but instead its details; the selectivity of the crystal rotation axis in the kink band is strongly affected by the loading orientation by varying the type of Burgers vector of the dislocations that construct the deformation kink band boundary.

4. Conclusions

(1) The frequency of formation of deformation bands in the LPSO-phase DS crystal monotonically decreases as the inclination angle of the loading axis with respect to the crystal growth direction increases, accompanied by a decrease in the yield stress.
(2) Deformation bands develop macroscopically along a direction approximately perpendicular to the grain boundary, which is parallel to (0001), independent of the loading orientation.
(3) The crystal rotation axis in the deformation bands is almost perpendicular to [0001] in almost all grains, independent of the loading orientation. However, the rotation axis varies between $\langle 10\bar{1}0\rangle$ and $\langle 2\bar{1}\bar{1}0\rangle$ on the [0001] zone axis, which depends on the loading axis in each grain.
(4) The observed features described above strongly suggest that the deformation bands formed in the LPSO phase are predominantly deformation kink bands.

Acknowledgments

This work was supported by JSPS KAKENHI for Scientific Research on Innovative Areas “MFS Materials Science (Grant Numbers: JP18H05478, JP18H05476 and JP18H05475)”, and KAKENHI JP18H05254. This work

was also partly supported by the Light Metals Educational Foundation of Japan.

REFERENCES

1) Y. Kawamura, K. Hayashi, A. Inoue and T. Masumoto: Mater. Trans. **42** (2001) 1172–1176.
2) M. Yamasaki, T. Anan, S. Yoshimoto and Y. Kawamura: Scr. Mater. **53** (2005) 799–803.
3) K. Hagihara, A. Kinoshita, Y. Sugino, M. Yamasaki, Y. Kawamura, H.Y. Yasuda and Y. Umakoshi: Acta Mater. **58** (2010) 6282–6293.
4) X.H. Shao, Z.Q. Yang and X.L. Ma: Acta Mater. **58** (2010) 4760–4771.
5) K. Hagihara, A. Kinoshita, Y. Sugino, M. Yamasaki, Y. Kawamura, H.Y. Yasuda and Y. Umakoshi: Intermetallics **18** (2010) 1079–1085.
6) M. Yamasaki, K. Hashimoto, K. Hagihara and Y. Kawamura: Acta Mater. **59** (2011) 3646–3658.
7) E. Oñorbe, G. Garcés, P. Pérez and P. Adeva: J. Mater. Sci. **47** (2012) 1085–1093.
8) J. Wang, P. Song, X. Zhou, X. Huang and F. Pan: Mater. Sci. Eng. A **556** (2012) 68–75.
9) K. Hagihara, A. Kinoshita, Y. Fukusumi, M. Yamasaki and Y. Kawamura: Mater. Sci. Eng. A **560** (2013) 71–79.
10) E. Oñorbe, G. Garcés, F. Dobes, P. Pérez and P. Adeva: Metall. Mater. Trans. A **44** (2013) 2869–2883.
11) L.B. Tong, X.H. Li and H.J. Zhang: Mater. Sci. Eng. A **563** (2013) 177–183.
12) G. Garces, P. Perez, S. Cabeza, H.K. Lin, S. Kim, W. Gan and P. Adeva: Mater. Sci. Eng. A **647** (2015) 287–293.
13) J.K. Kim, S. Sandlöbes and D. Raabe: Acta Mater. **82** (2015) 414–423.
14) H. Liu, J. Bai, K. Yan, J. Yan, A. Ma and J. Jiang: Mater. Des. **93** (2016) 9–18.
15) G. Garcés, K. Máthis, J. Medina, K. Horváth, D. Drozdenko, E. Oñorbe, P. Dobroň, P. Pérez, M. Klaus and P. Adeva: Int. J. Plast. **106** (2018) 107–128.
16) K. Hagihara, Z. Li, M. Yamasaki, Y. Kawamura and T. Nakano: Acta Mater. **163** (2019) 226–239.
17) K. Hagihara, N. Yokotani and Y. Umakoshi: Intermetallics **18** (2010) 267–276.
18) K. Hagihara, Y. Sugino, Y. Fukusumi, Y. Umakoshi and T. Nakano: Mater. Trans. **52** (2011) 1096–1103.
19) K. Hagihara, Y. Fukusumi, M. Yamasaki, T. Nakano and Y. Kawamura: Mater. Trans. **54** (2013) 693–697.
20) K. Hagihara, T. Okamoto, H. Izuno, M. Yamasaki, M. Matsushita, T. Nakano and Y. Kawamura: Acta Mater. **109** (2016) 90–102.
21) J.B. Hess and C.S. Barrett: Trans. Am. Inst. Min. Met. Eng. **185** (1949) 599–606.
22) M. Yamasaki, K. Hagihara, S. Inoue, J.P. Hadorn and K. Kawamura: Acta Mater. **61** (2013) 2065–2076.
23) K. Hagihara, M. Yamasaki, M. Honnami, H. Izuno, M. Tane, T. Nakano and Y. Kawamura: Philos. Mag. **95** (2015) 132–157.
24) X.H. Shao, Z.Z. Peng, Q.Q. Jin and X.L. Ma: Acta Mater. **118** (2016) 177–186.
25) K. Hagihara, T. Okamoto, M. Yamasaki, Y. Kawamura and T. Nakano: Scr. Mater. **117** (2016) 32–36.
26) Z.Z. Peng, X.H. Shao, Q.Q. Jin, J.F. Liu and X.L. Ma: Mater. Sci. Eng. A **687** (2017) 211–220.
27) T. Matsumoto, M. Yamasaki, K. Hagihara and Y. Kawamura: Acta Mater. **151** (2018) 112–124.
28) K. Kishida, A. Inoue, H. Yokobayashi and H. Inui: Scr. Mater. **89** (2014) 25–28.
29) Y. Mine, R. Maezono, H. Oda, M. Yamasaki, Y. Kawamura and K. Takashima: Mater. Trans. **56** (2015) 952–956.
30) C.A. Schneider, W.S. Rasband and K.W. Eliceiri: Nat. Methods **9** (2012) 671–675.
31) A. Inoue, K. Kishida, H. Inui and K. Hagihara: MRS Symp. Proc. **1516** (2013) 151–156.
32) K. Hagihara, T. Mayama, M. Honnami, M. Yamasaki, H. Izuno, T. Okamoto, T. Ohashi, T. Nakano and Y. Kawamura: Int. J. Plast. **77** (2016) 174–191.